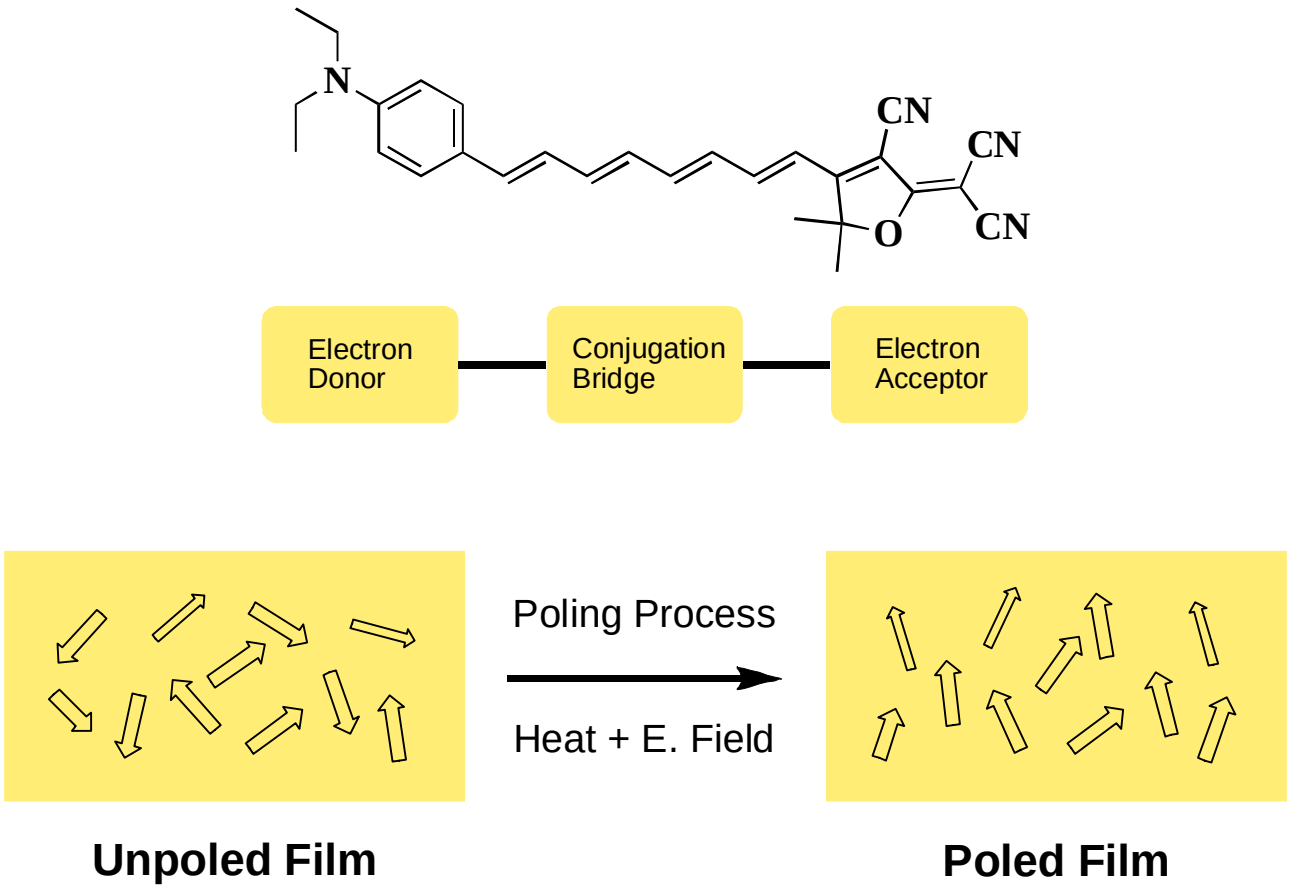

FIGURE 16.1 Illustration of static electric field poling process of dipolar nonlinear optical (NLO) chromophores doped in a supporting polymer matrix. Before applying electric field the dipole moments are randomly distributed. At near glass transition temperature the dipole moments of NLO chromophores are mobile and respond to the direction of the applied external field. The orientation of chromophore is frozen-in by cooling to low temperature to form a poled polymer with noncentrosymmetric distribution of dipolar NLO chromophores.

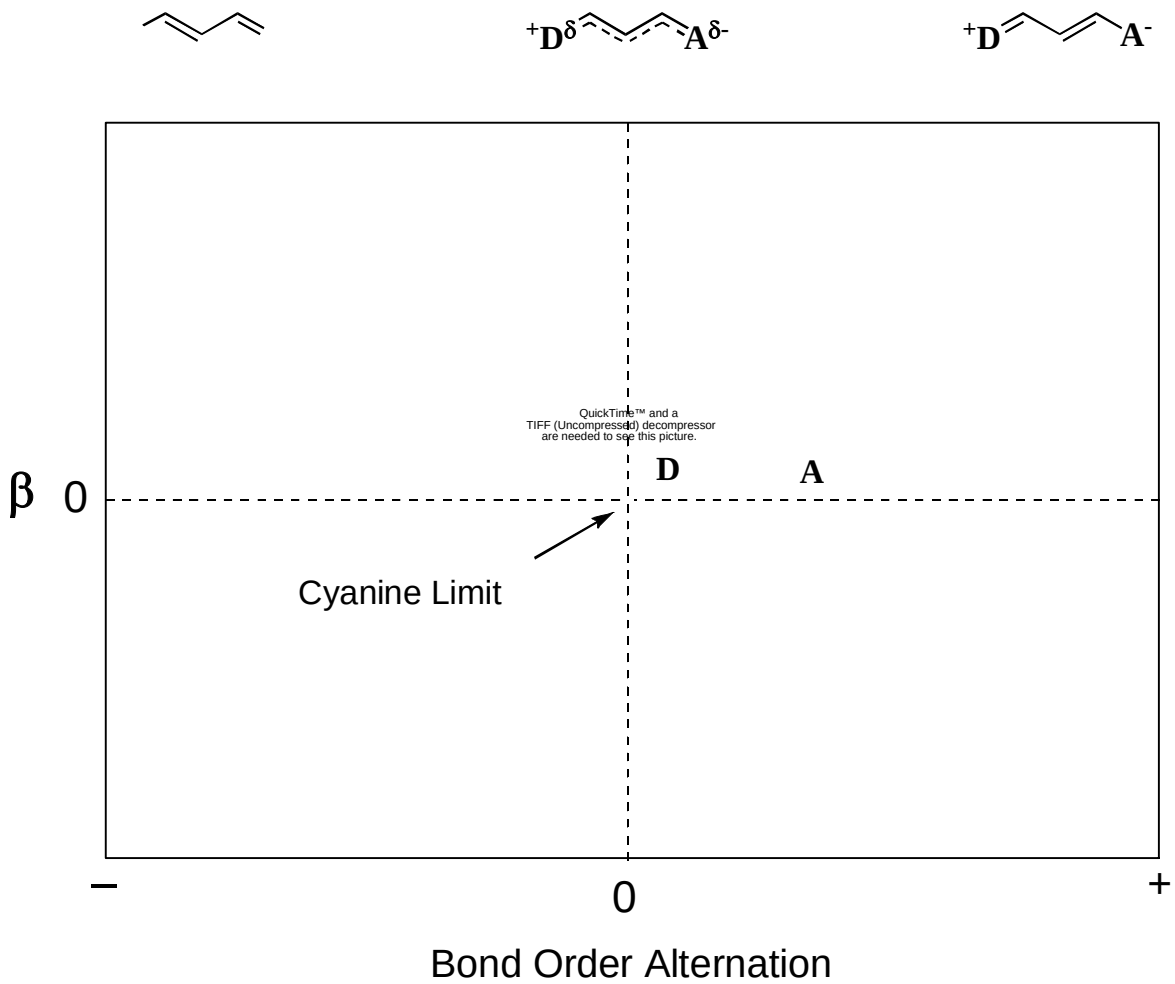

FIGURE 16.2 Schematic plot showing how dispersion-free molecular hyperpolarizability varies with bond order alternation (BOA or bond length alternation, BLA) for a donor-bridge-acceptor chromophore, along with the variation (resonance structures) of the constituent terms.

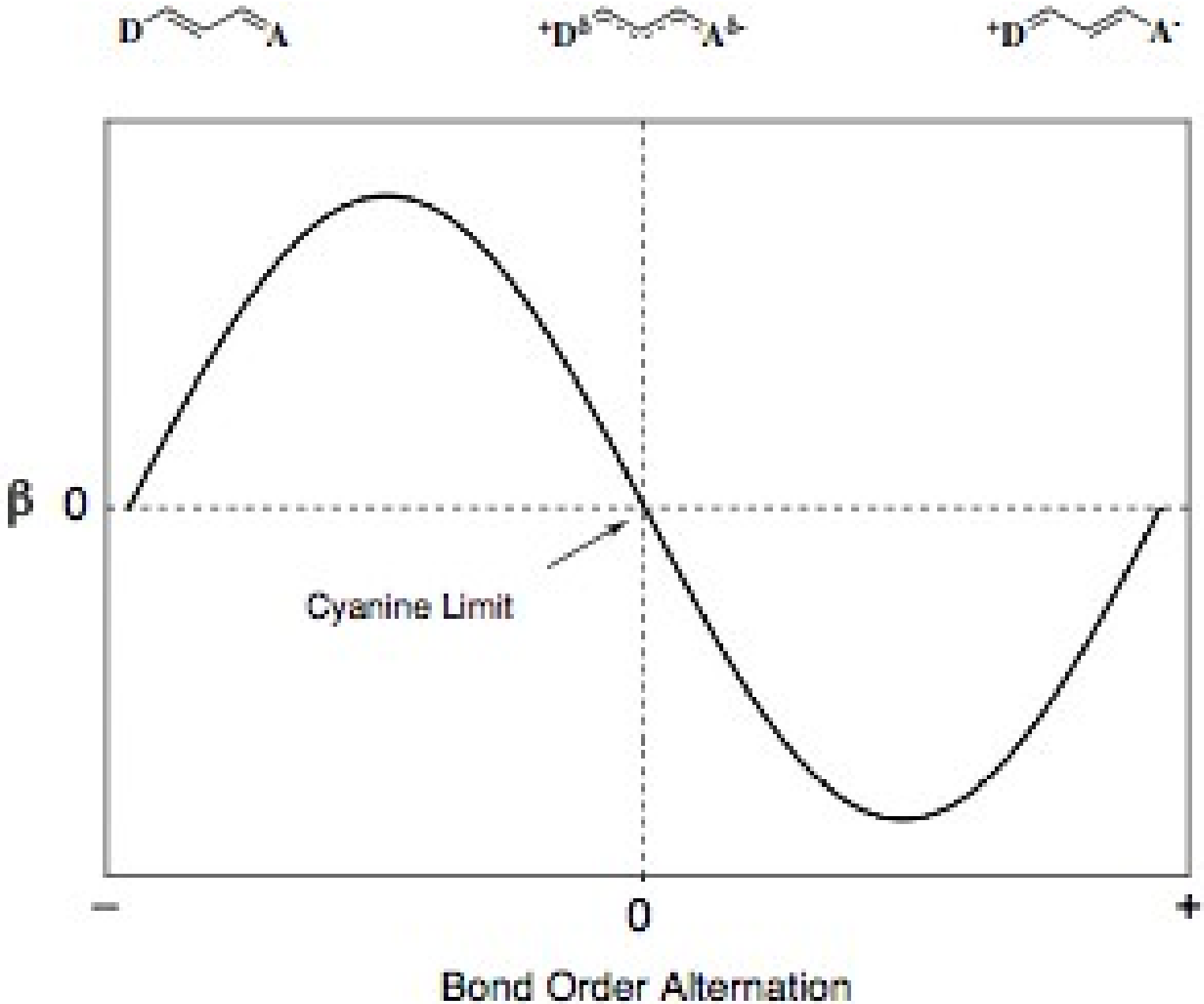
D
A
+Dδ
Aδ-
+D
A-
β
0
Cyanine Limit
−
0
+
Bond Order Alternation

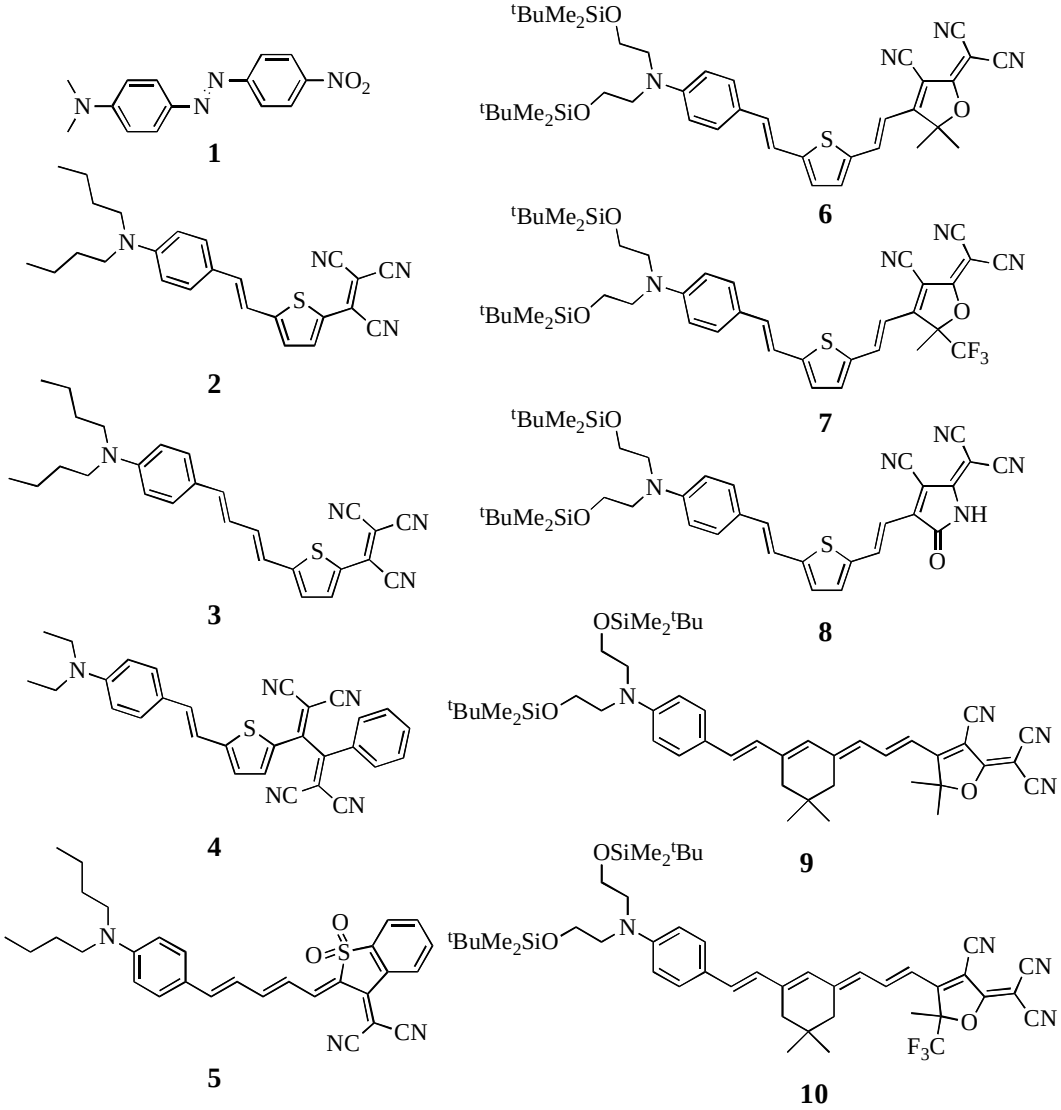

FIGURE 16.3 Molecular structures of representative dipolar NLO chromophores.

Introduction to Organic Electronic and Optoelectronic Materials and Devices (Eds. Sun & Dalton) CRC Press, 2008. ISBN-10: 0849392845

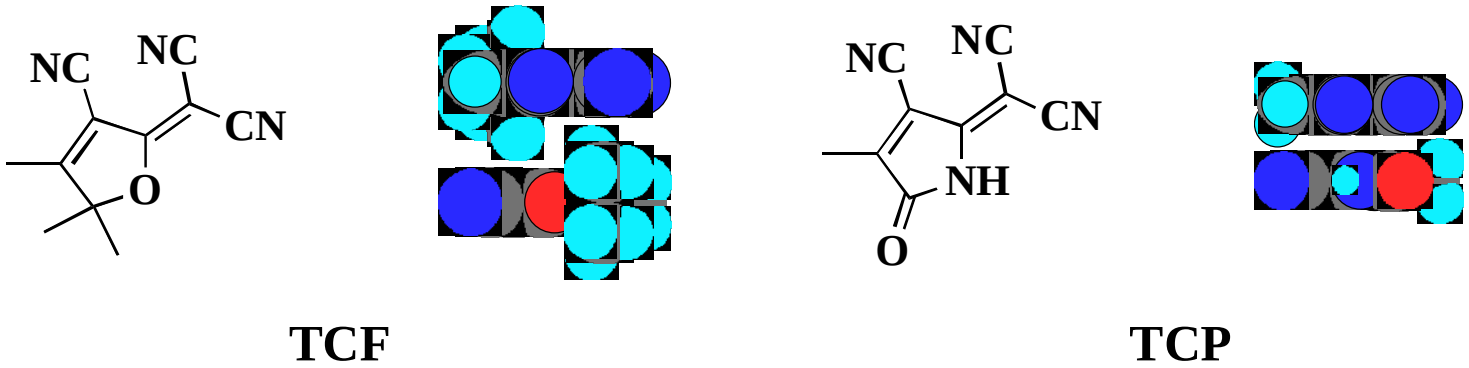

FIGURE 16.4 Structural differences between acceptors are shown. In TCF acceptor geminal dimethyl groups act as spacers above and below the π-electron plane. The electrostatic dipole–dipole interactions between acceptors in dimers in TCF acceptor are expected to be weaker and easier to reorient by electric field poling compare to fl at TCP acceptor.

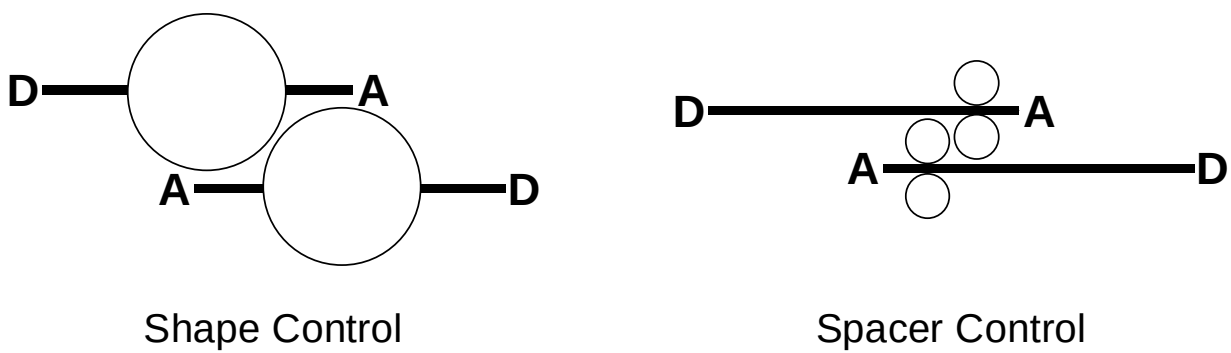

FIGURE 16.5 Schematic comparison of the shape control and spacer control. Notice that the use of small but efficient spacers above and blow the plane of π-conjugation system can prevent the electrostatic Intermolecular interactions effectively and lower the aggregation energy with minimal addition to the passive volume of chromophores.

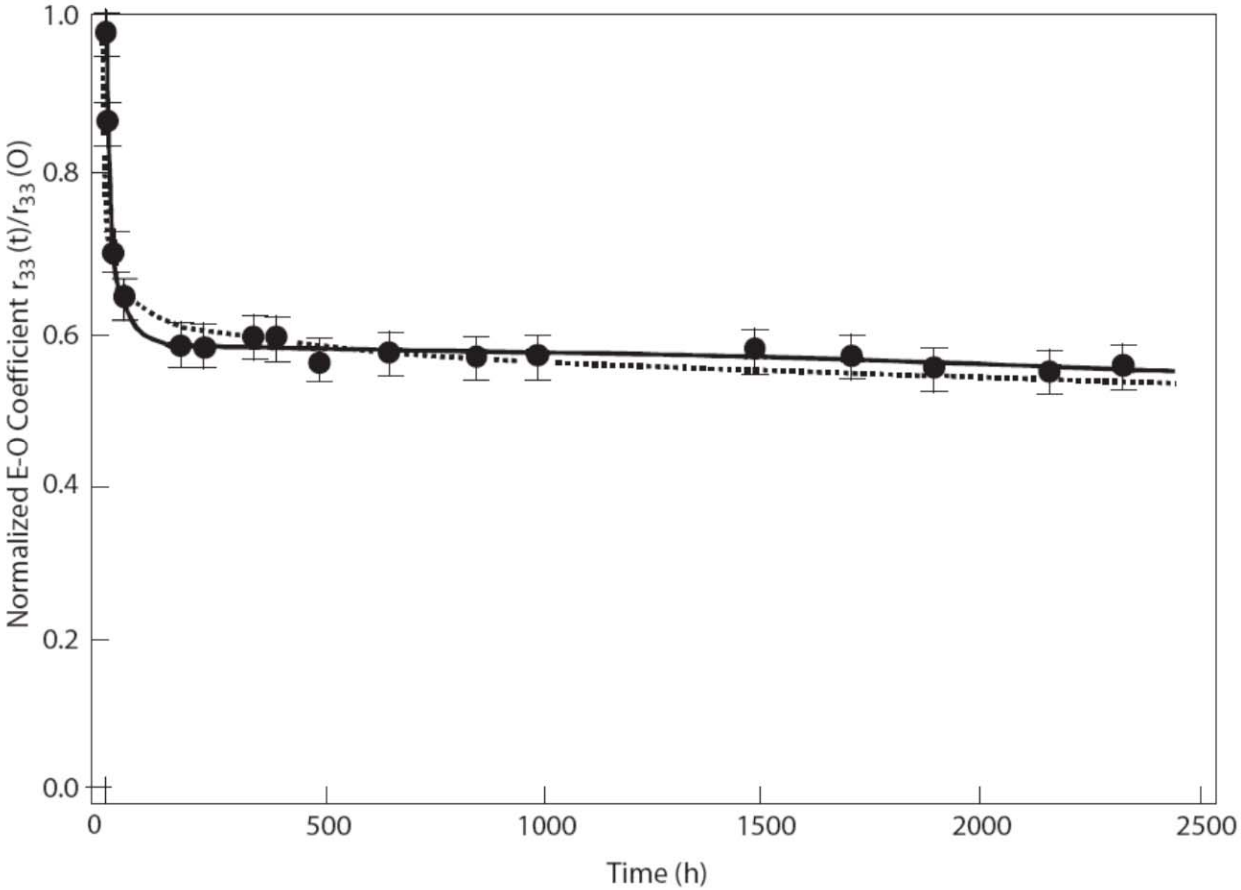

FIGURE 16.6 Normalized E-O coefficient of guest–host polymer of chromophore **3** at 80° C.

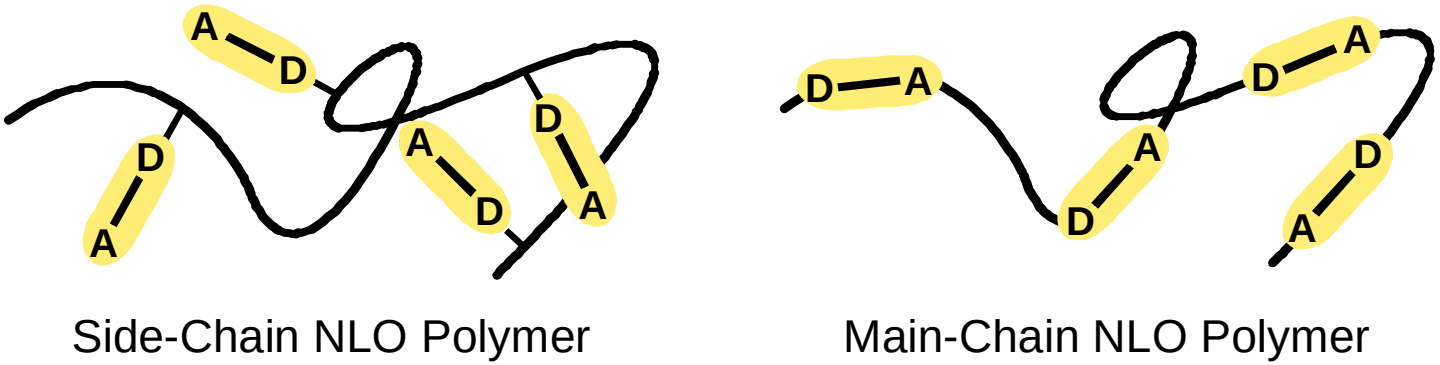

FIGURE 16.7 Schematic comparison of the side-chain and main-chain NLO polymers.

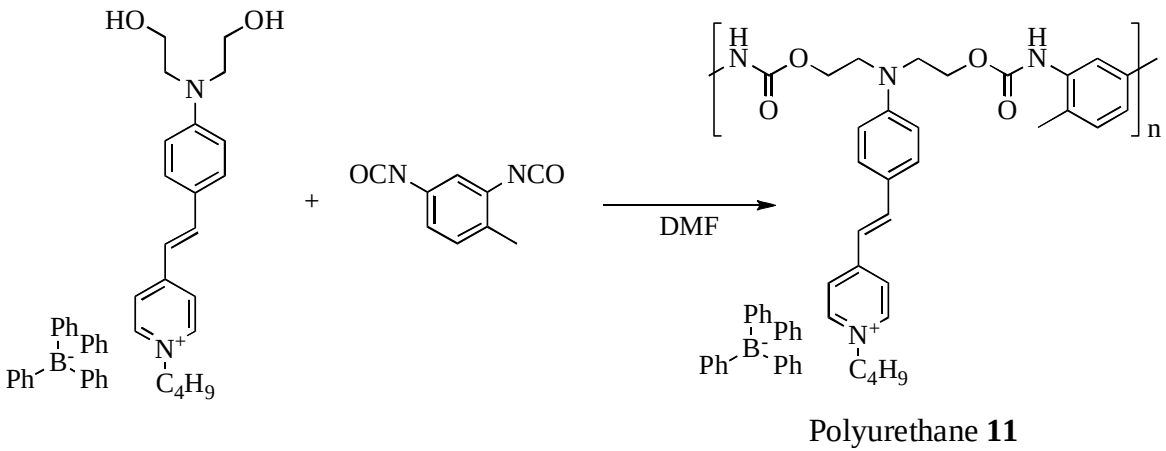

FIGURE 16.8 Synthesis of polyurethane by step-growth polymerization.

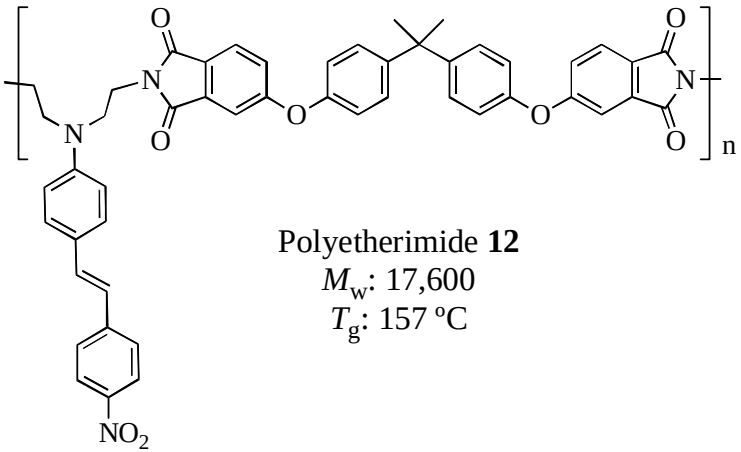

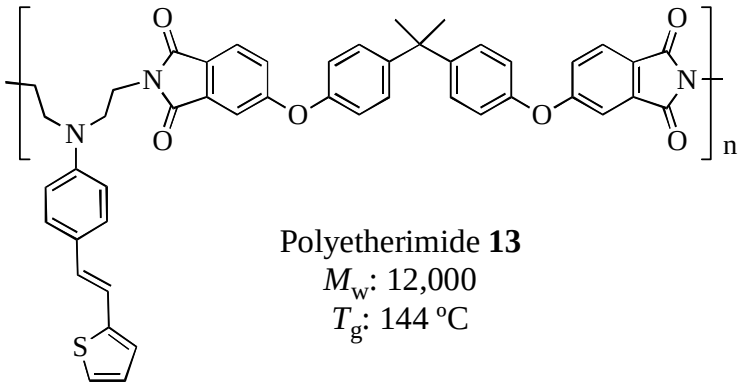

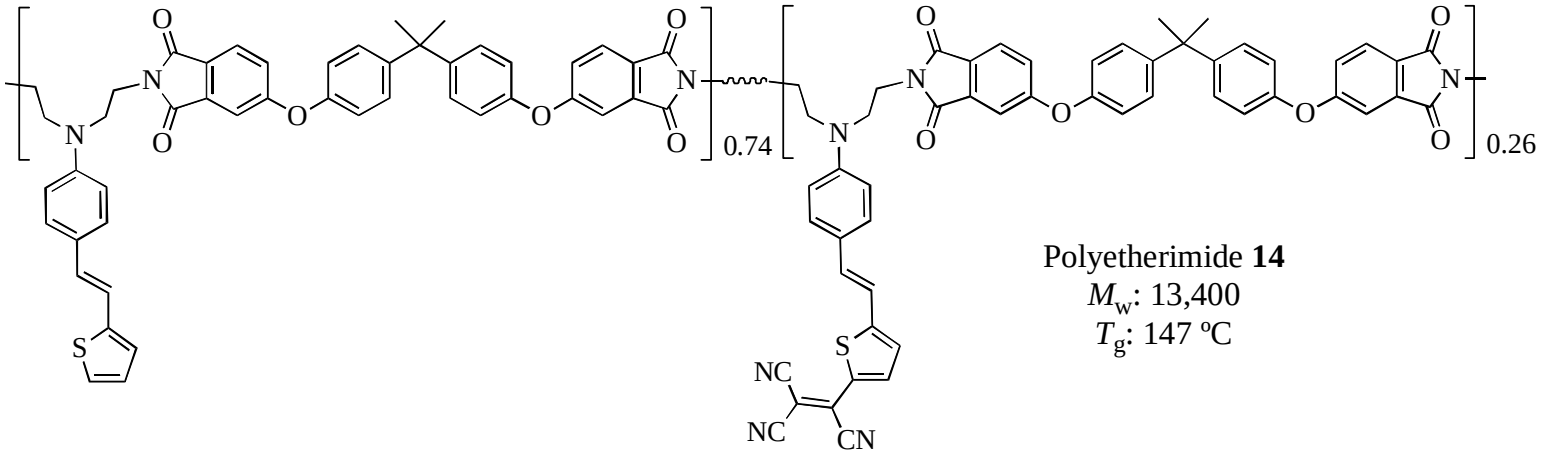

FIGURE 16.9 Structures of PEIs **12**–**14**. Note the PEI **14** is prepared from the PEI **13** by a post-functionalization reaction, tricyano-vinylation.

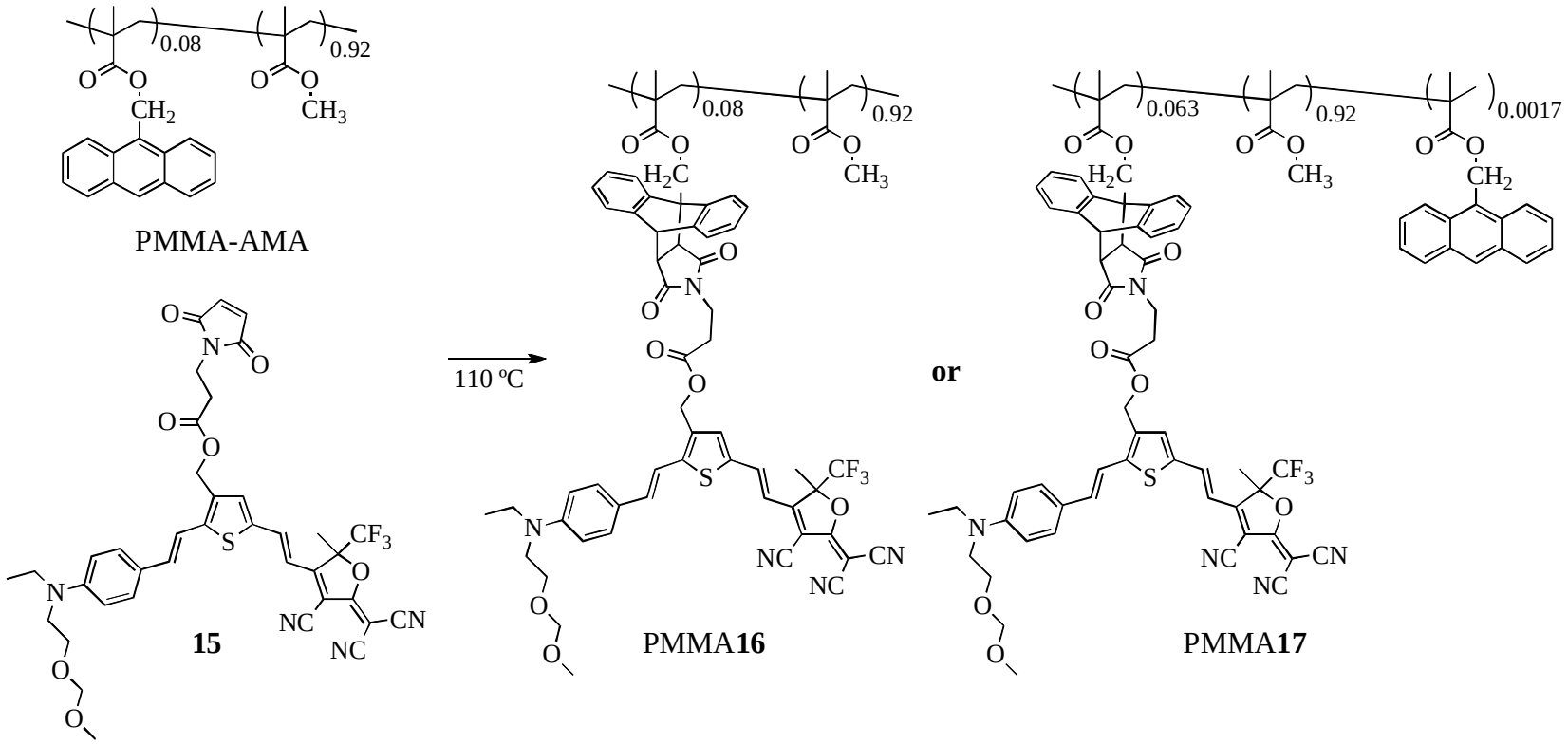

FIGURE 16.10 Synthetic procedures for side-chain NLO polymers PMMA **16** and PMMA **17** by a postfunctionalization, D–A reaction.

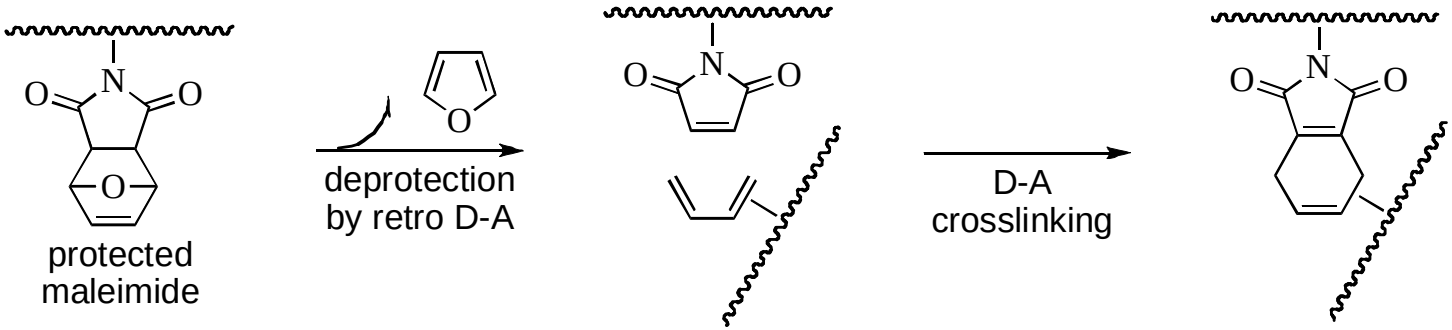

FIGURE 16.11 Reaction sequences of D–A cross-linking (or lattice-hardening) process.

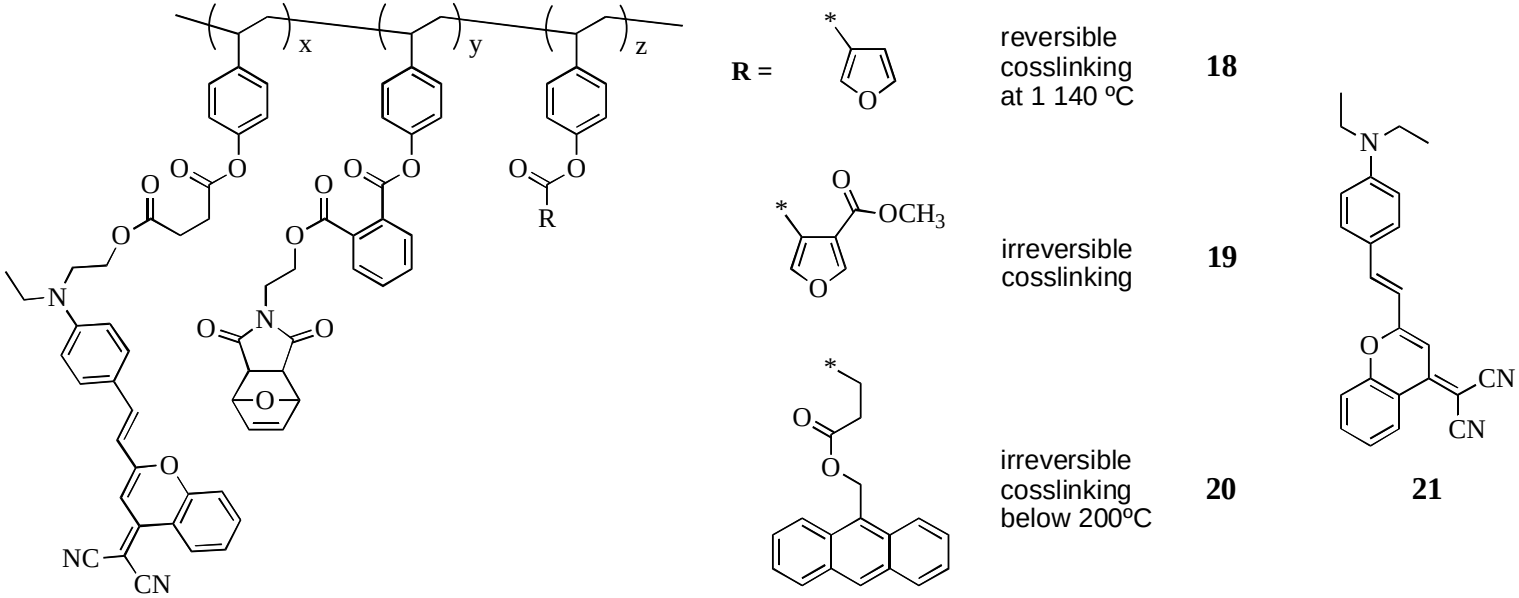

FIGURE 16.12 Molecular structures of side-chain NLO polymers with D–A cross-linkers **18**–**20** and a chromone derivative **21**.

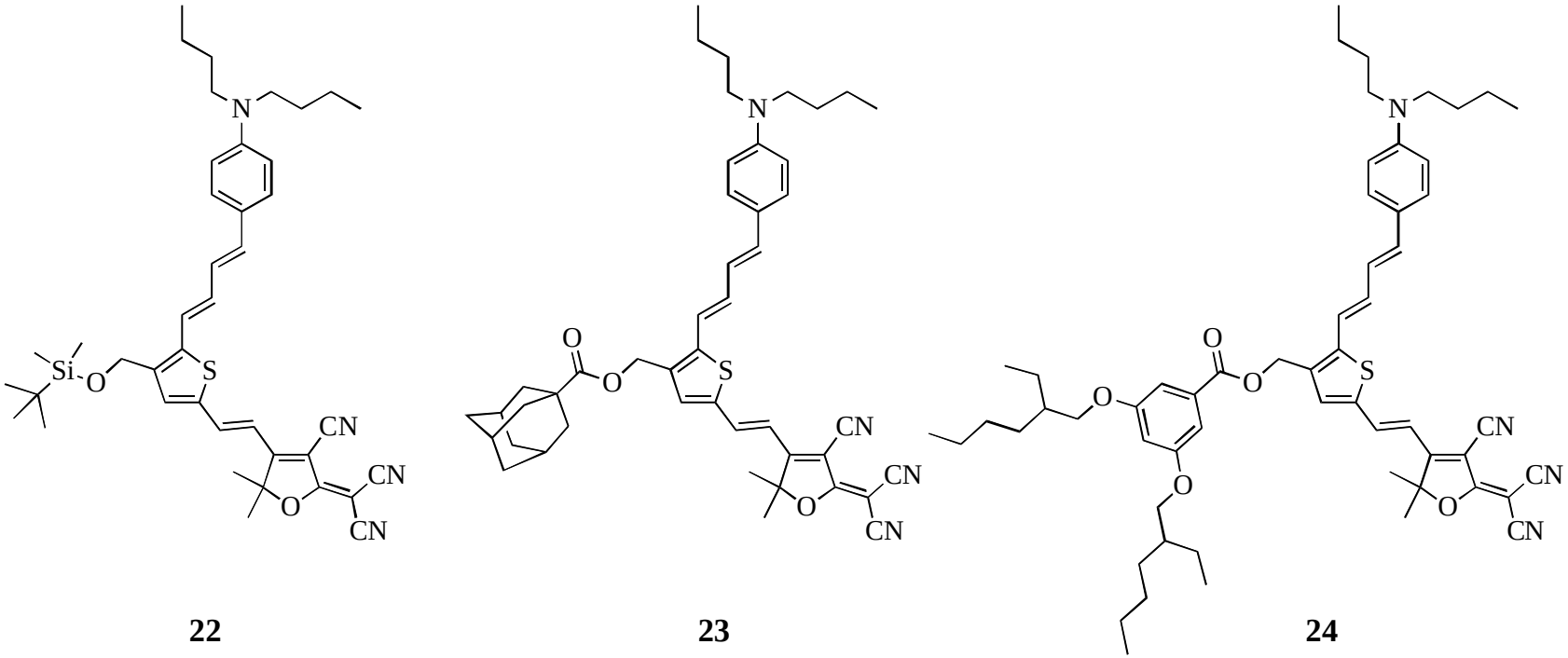

FIGURE 16.13 Molecular structures of shape modified NLO chromophores **22**-**24**.

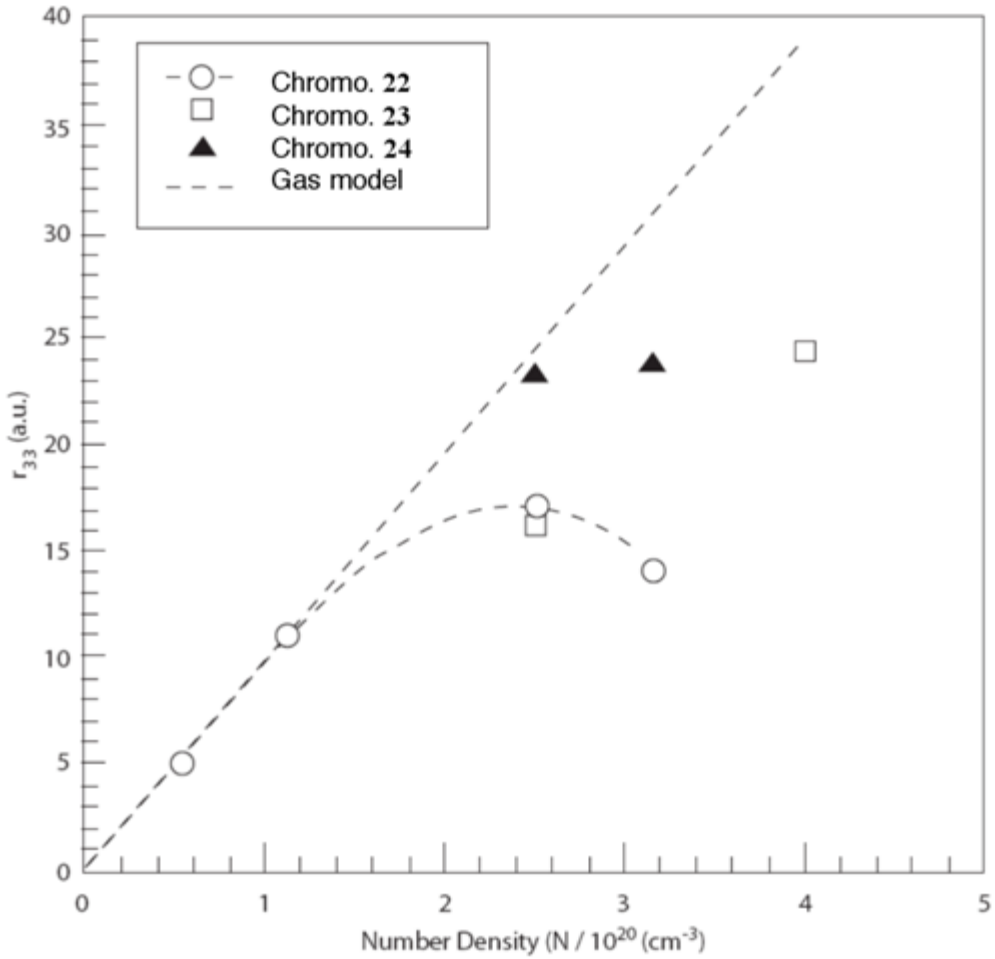

FIGURE 16.14 Comparison on E-O coefficient of NLO polymers incorporated with chromophores Containing different loading density and substituents.

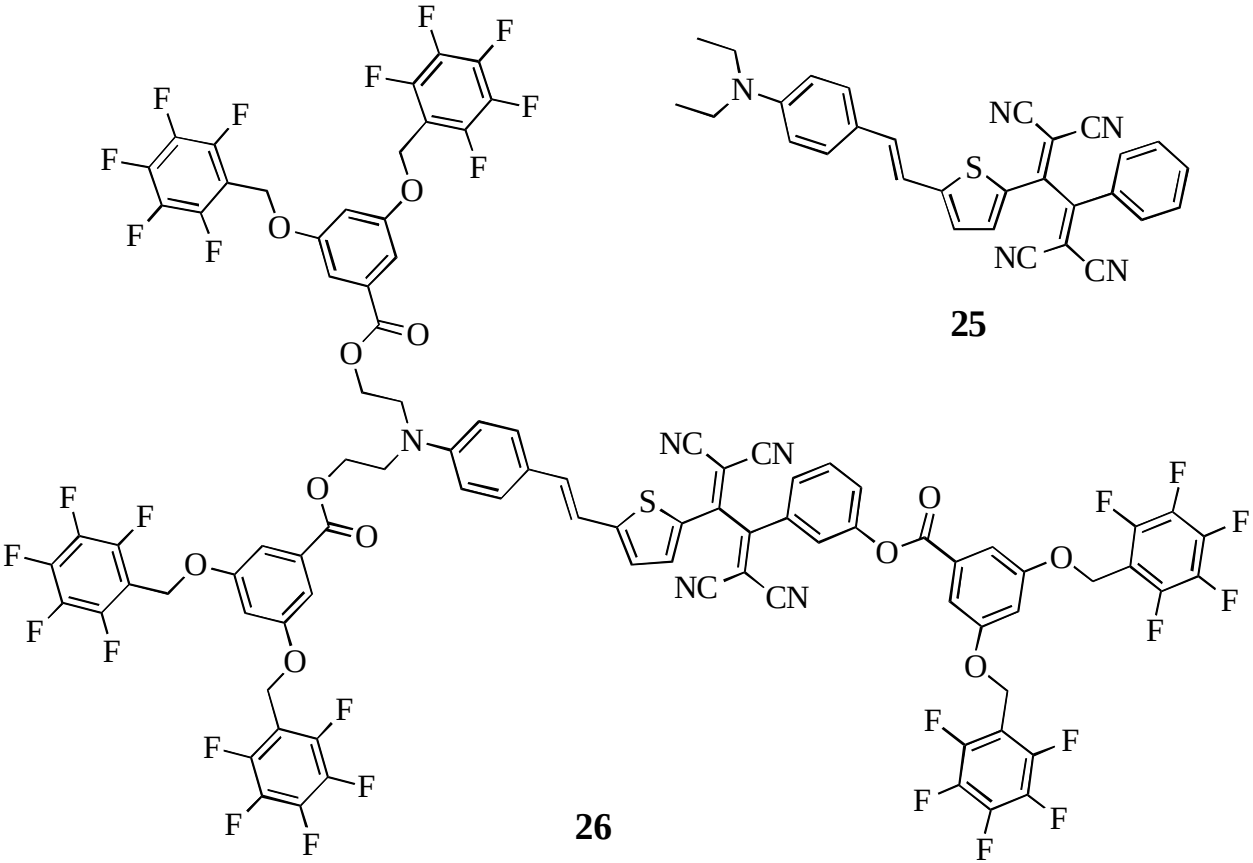

FIGURE 16.15 Molecular structures of non-dendronized chromophore **25** and dendronized chromophore **26**.

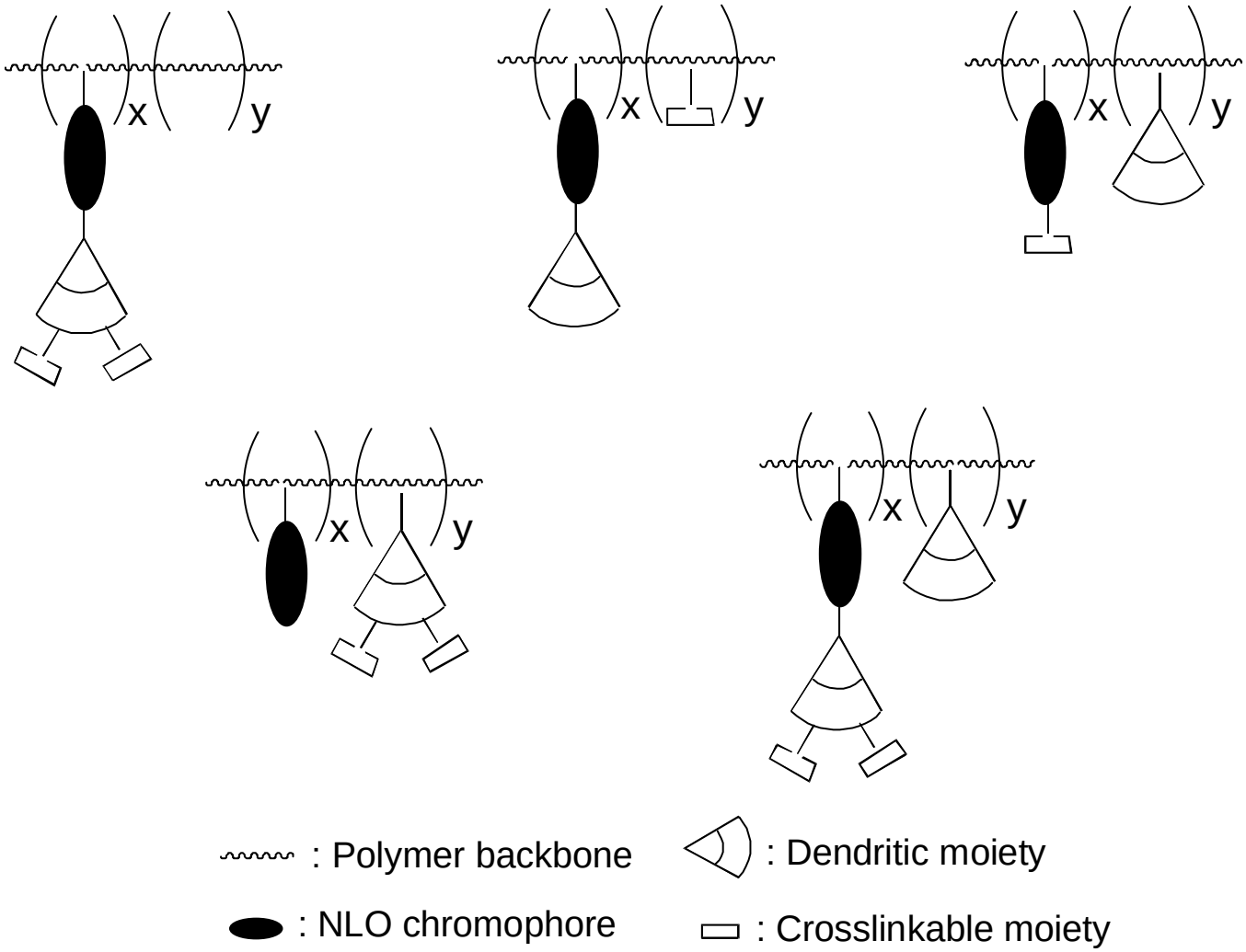

FIGURE 16.16 Molecular architectures of dendronized side-chain NLO polymers with cross-linkers.

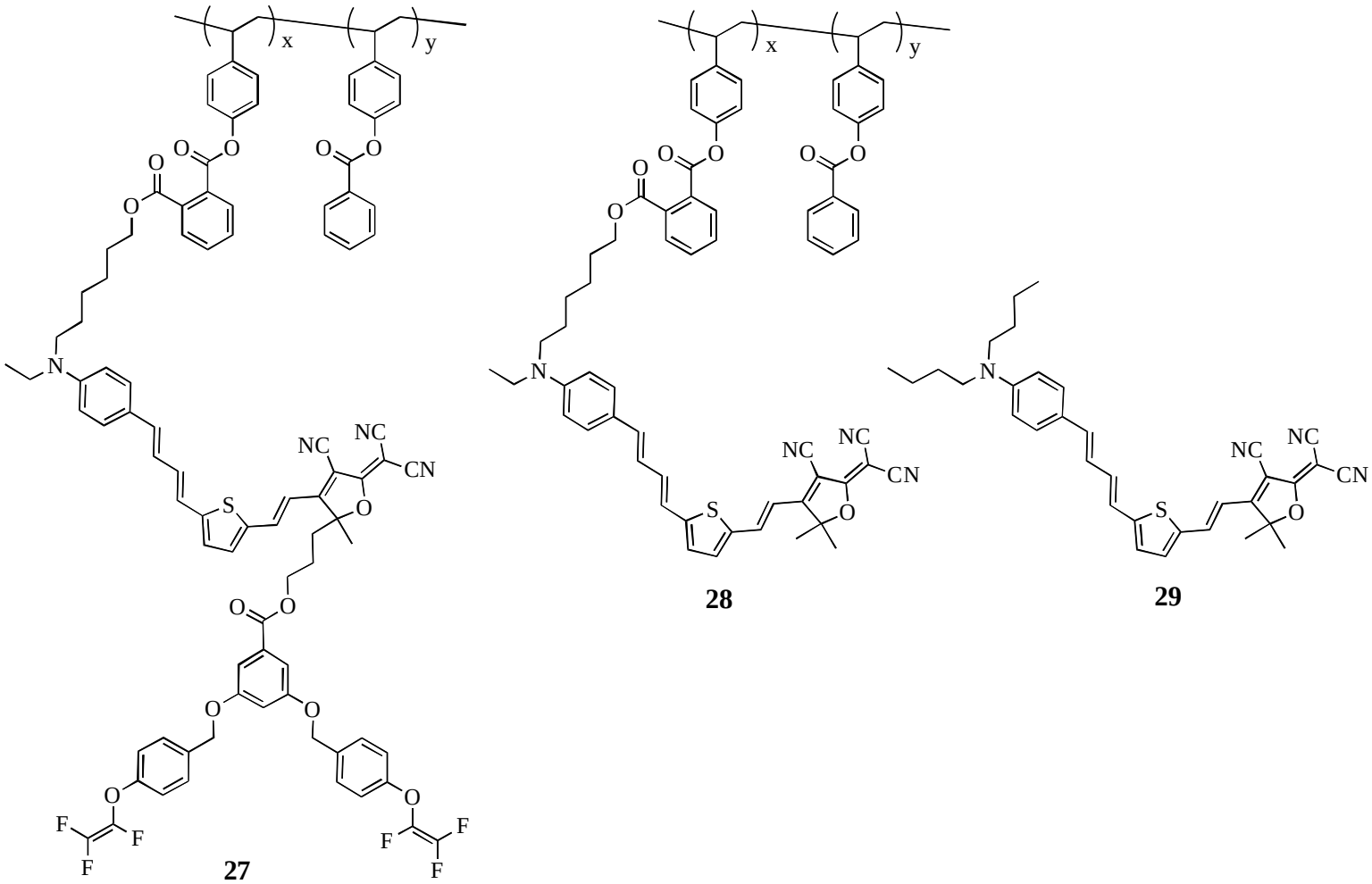

FIGURE 16.17 Molecular structures of dendronized side-chain NLO polystyrene **27** with partially fluorinated dendrons, conventional side-chain polystyrene **28**, and the core chromophore **29**.

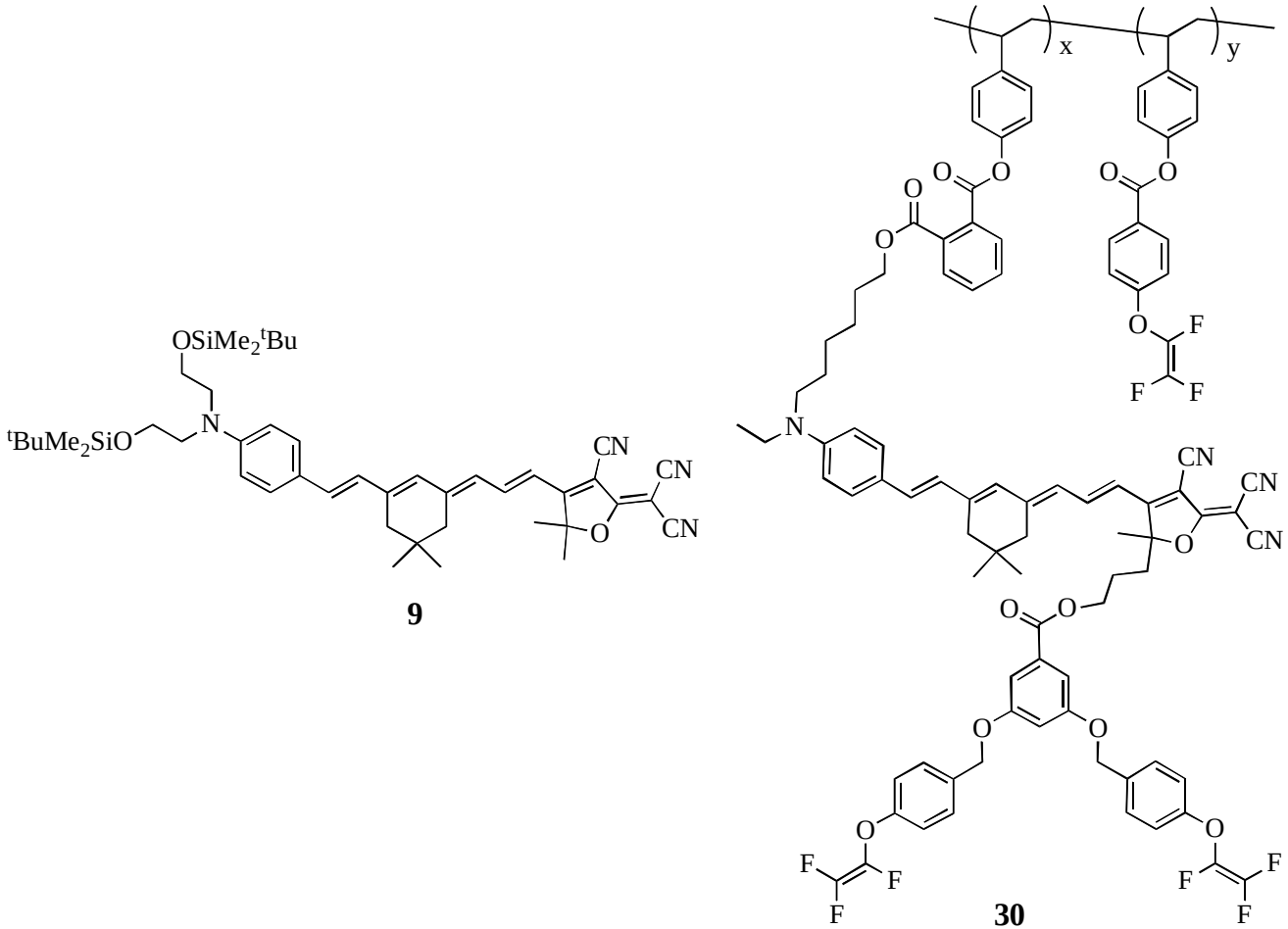

FIGURE 16.18 Molecular structures of the core chromophore **9** and side-chain polystyrene **30** having Chromophore modified with partially fluorinated dendron.

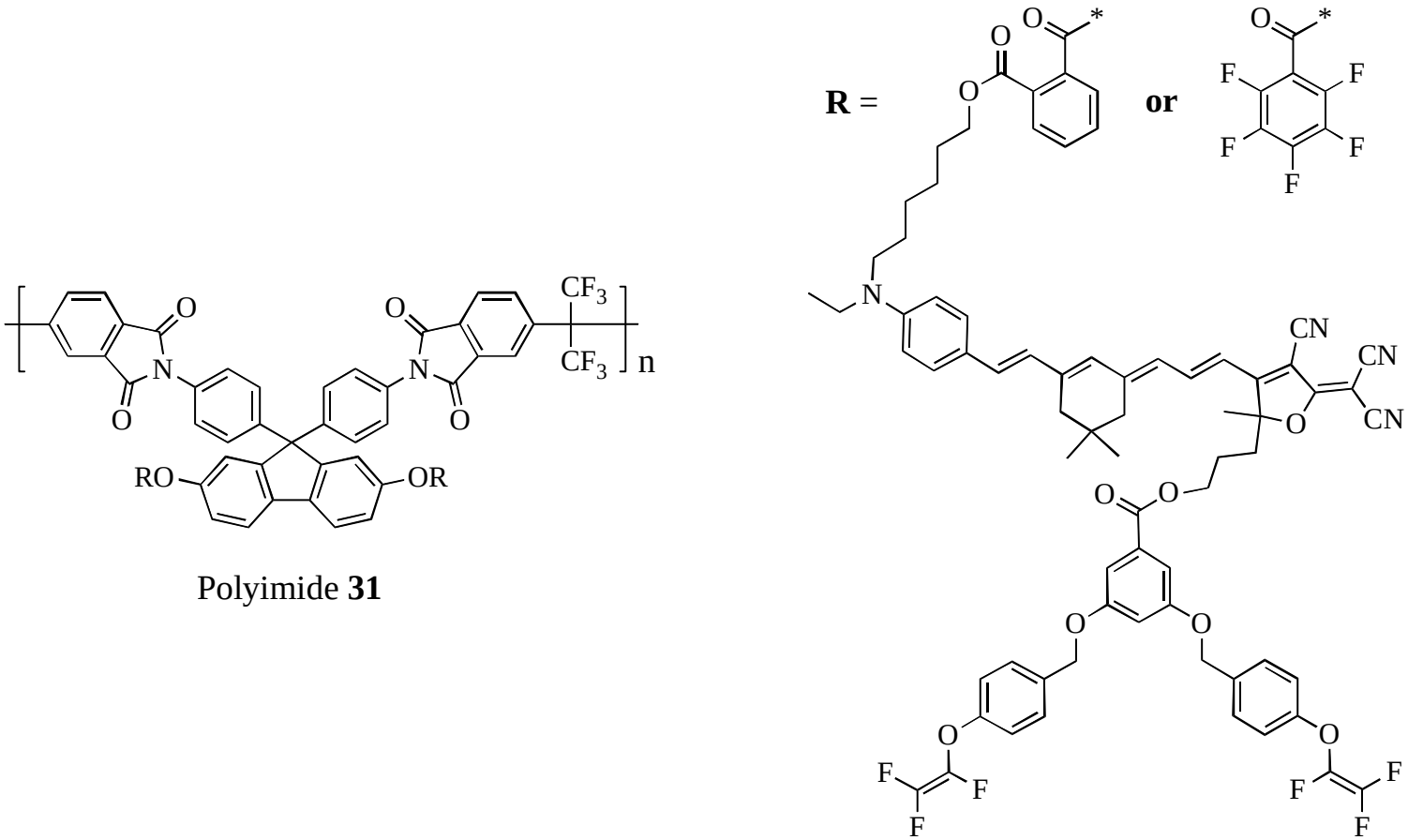

FIGURE 16.19 Molecular structure of a high Tg aromatic side-chain polyimide **31** with dendronized NLO chromophores as pendant groups.

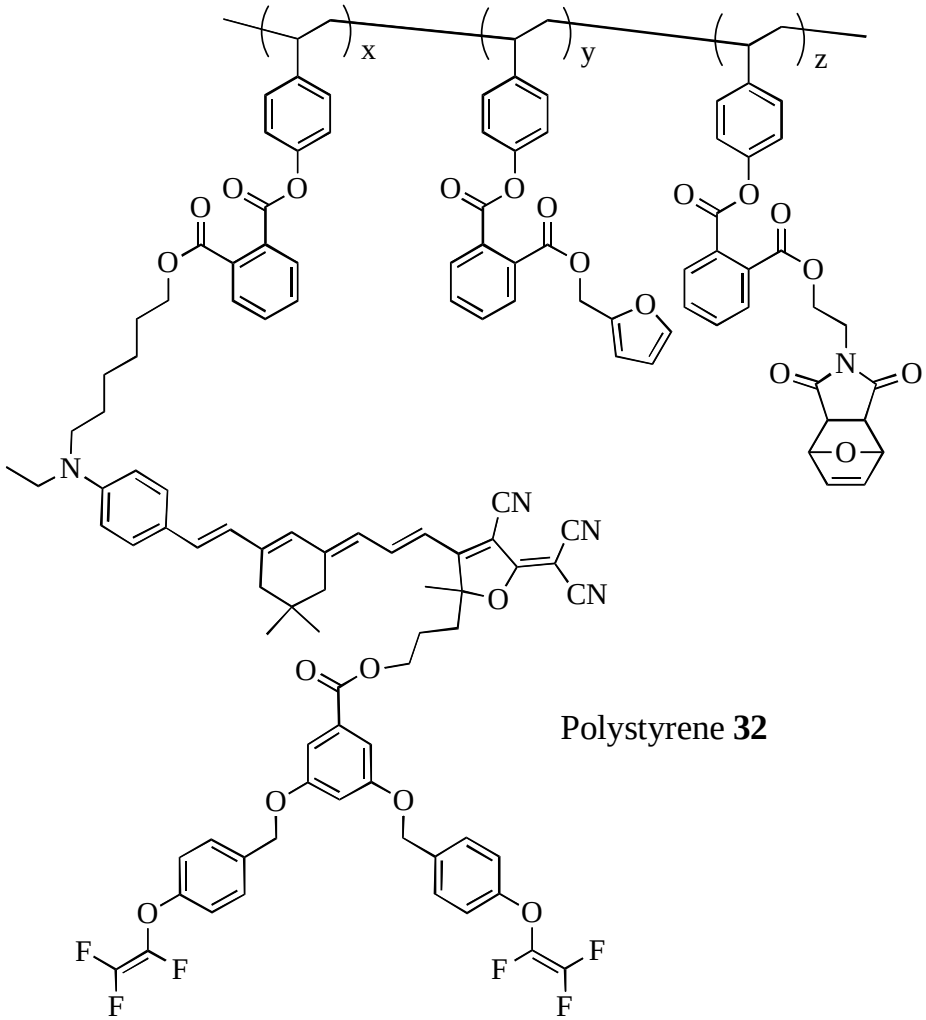

FIGURE 16.20 Molecular structure of side-chain polystyrene **32** with D–A cross-linker and fluorinated dendron.

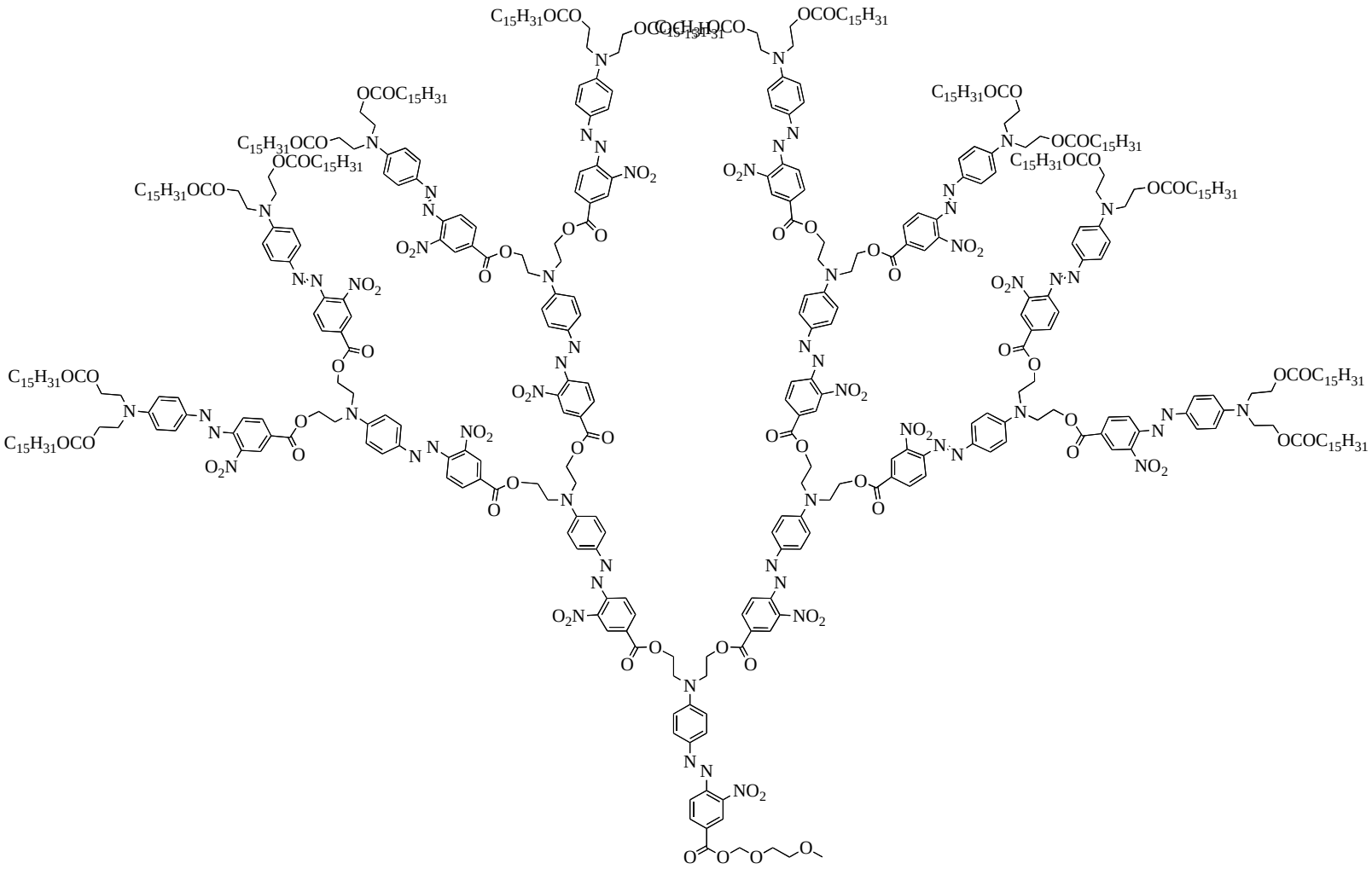

FIGURE 16.21 Molecular structure of a dendrimer **33** in a spreading shape.

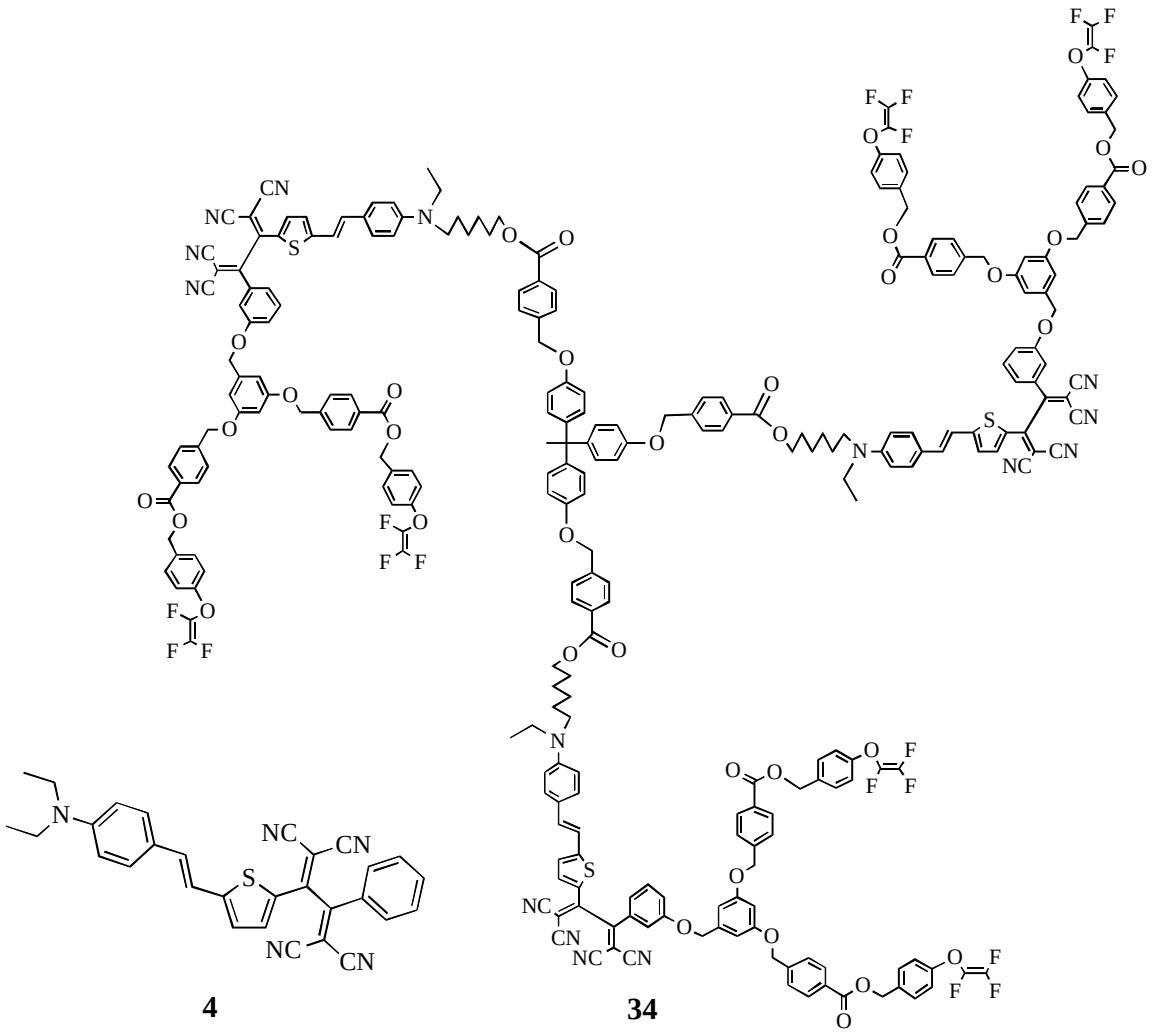

FIGURE 16.22 Molecular structure of dendron **34** (*Mw* = 4664 Da, chromophore density: 33 wt %).

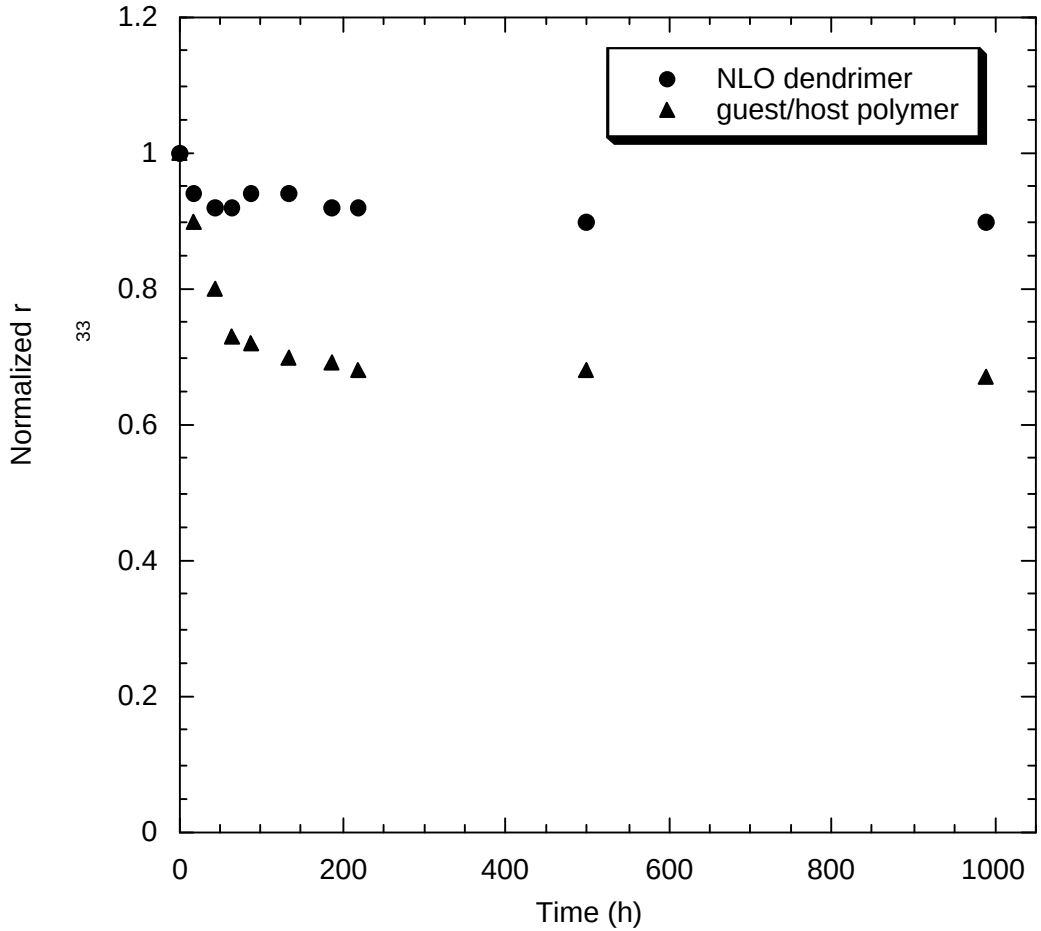

FIGURE 16.23 Temporal stability of the post-poling cross-linked NLO dendrimer **34**, and a guest–host polymer in PQ-100 at 85° C under nitrogen. The r_{33} values were normalized as a function of time.

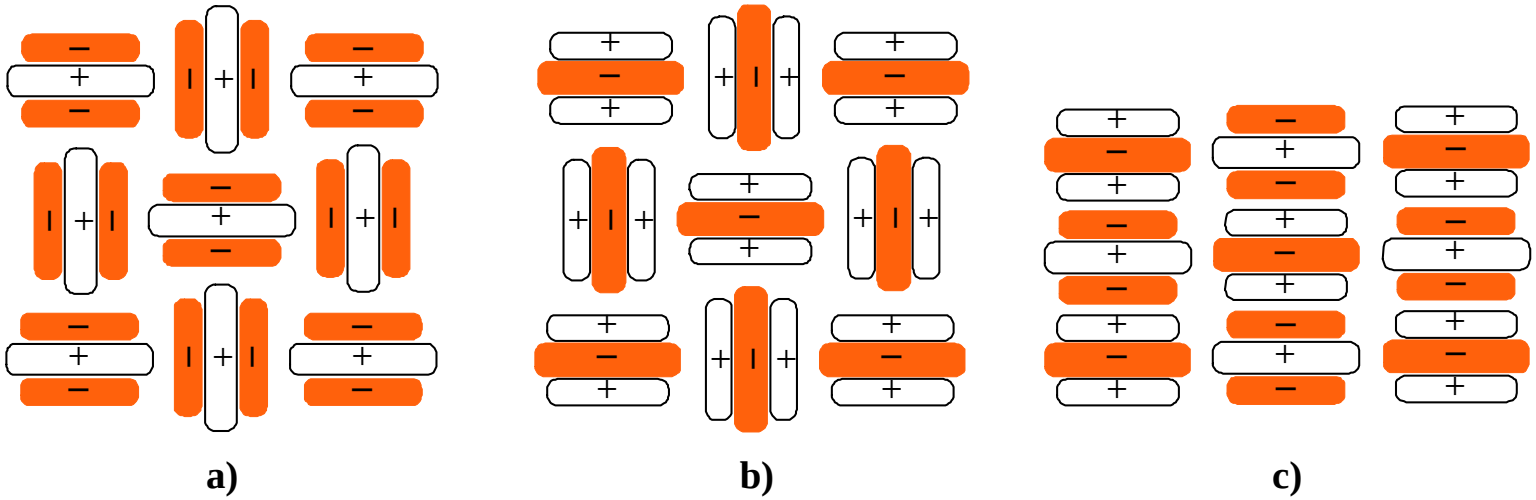

FIGURE 16.24 The Ar–Ar^F interactions in the crystal of (a) benzene; (b) hexafluorobenzene; and (c) alternating stacks of benzene-hexafluorobenzene co-crystal.

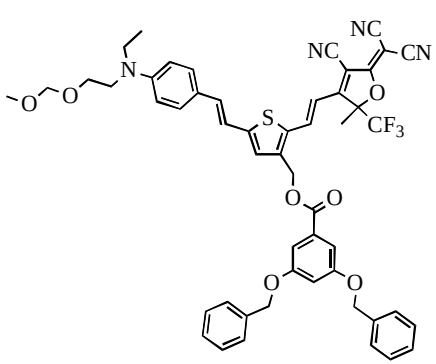

35

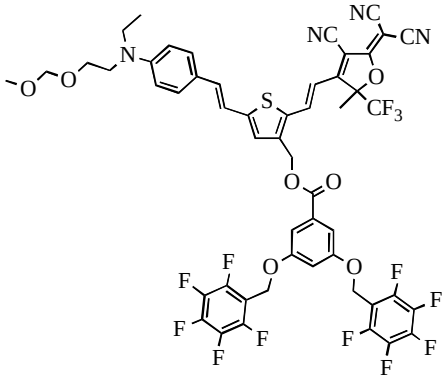

36

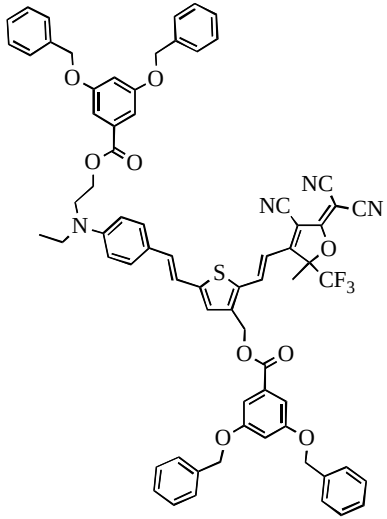

37

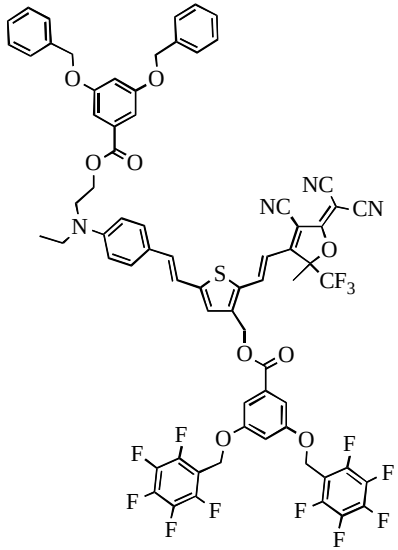

38

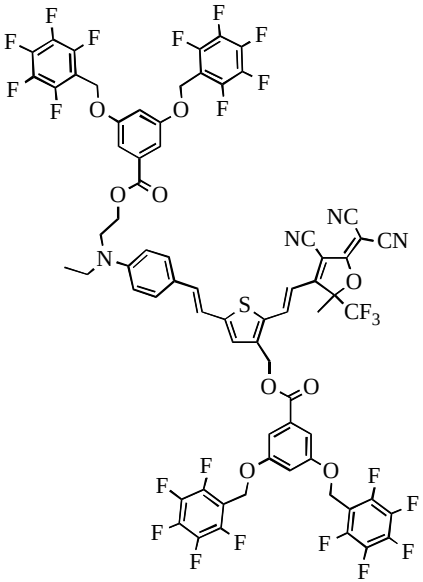

39

FIGURE 16.25 Molecular structure of chromophores used for the reversible self-assembly of supramolecular glasses.

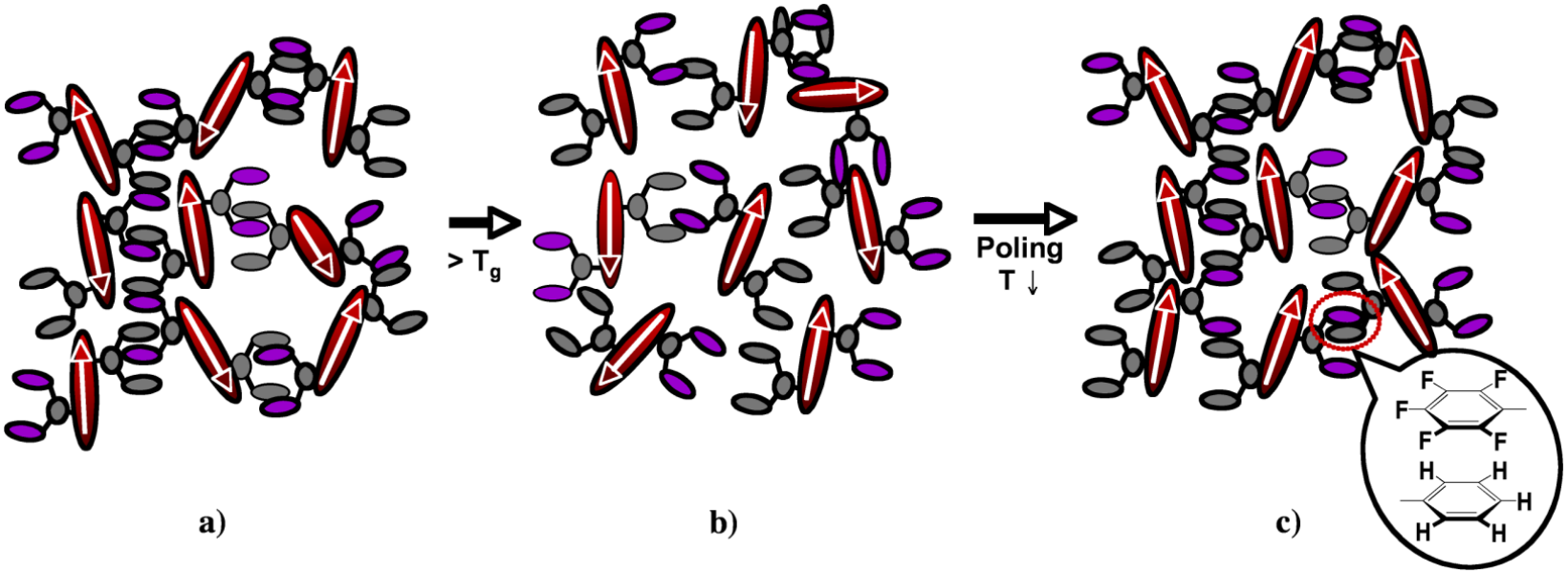

FIGURE 16.26 Graphical illustration of material processing sequences to generate the macroscopic noncentrosymmetric order of supramolecular self-assembly of chromophore glasses by Ar–Ar^F interactions and electric field poling. (a) glassy supramolecular self-assembly of chromophores with random dipoles (shown as arrows) before poling (b) mobile rubbery state with random dipoles before poling (c) glassy supramolecular self-assembly of chromophores with noncentrosymmetric dipoles after poling followed by cooling.

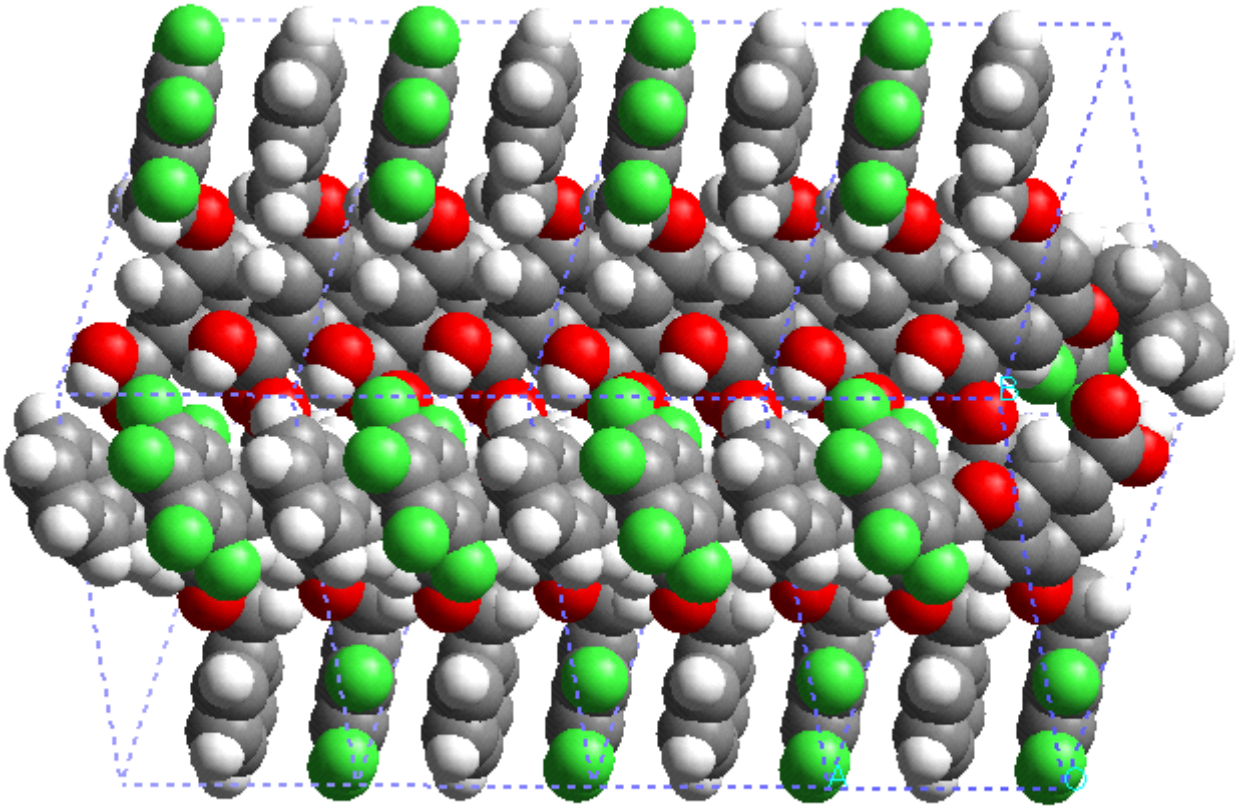

FIGURE 16.27 A space filling structure of alternating co-crystal stacks of hetero-dimer.

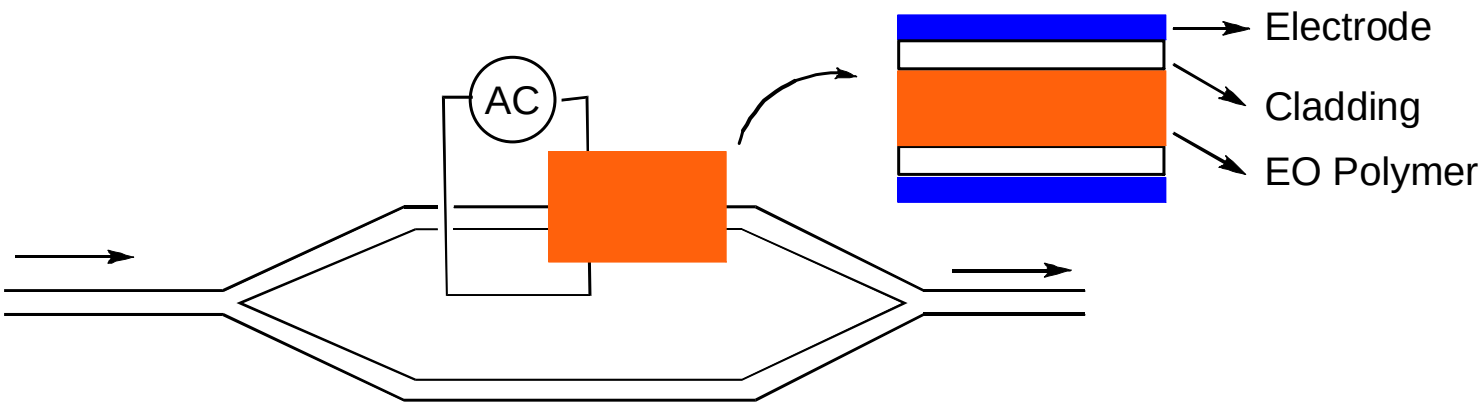

FIGURE 16.28 Schematic representation of the structure of a Mach–Zehnder interferometer for amplitude modulation.